Available online at www.sciencedirect.com
SCIENCE DIRECT®
Thermochimica Acta 409 (2004) 111–119
thermochimica acta
www.elsevier.com/locate/tca

Comparison of simulated and actual DSC measurements for first-order transitions

Robert L. Danley*

TA Instruments, 109 Lukens Drive, New Castle, DE 19720, USA

Received 3 December 2002; received in revised form 10 June 2003; accepted 11 June 2003

Abstract

A system of differential equations modeling a heat flux DSC is solved and the results are compared with those obtained using a TA Instruments Q1000™ DSC.[1] It incorporates a new heat flow rate measurement technique that determines the heat flow rate between the sample and its pan. Two types of first-order transitions are investigated: melting of a pure substance and solidification of a pure substance including super-cooling. In both transitions, the peak shape obtained using the new heat flow rate measurement and predicted by the model is quite different from that measured using conventional DSC. It is shown that the differences are the result of simplifications implicit in the conventional heat flow rate measurement that is based solely on the difference between sample and reference calorimeter temperatures. Heat flow rates measured using the improved measurement agree very well with the model predictions for heat exchange between the sample and its pan.

Keywords: DSC thermal model; Heat flow rate measurement; First-order transition

1. Introduction

Differential scanning calorimetry is a widely used analytical technique where the heat flow rate to a sample under analysis is measured while the temperature of the instrument is controlled to follow a desired program. It is a twin instrument comprising sample and reference calorimeters that are essentially identical. In the vast majority of DSCs the measured signal is the difference between the sample and reference calorimeter temperatures, which is converted into the sample heat flow rate by multiplying the signal by a temperature-dependent proportionality factor. However, it is well known that the resulting heat flow rate signal during a transition is an inexact representation of the actual sample heat flow rate. The measured heat flow rate is delayed and distorted in time [1]. This distortion or smearing of the heat flow rate is the result of lags due to heat capacities and thermal resistances in the apparatus.

The DSC literature is replete with descriptions of various models of the DSC measurement apparatus [2–20]. Even before the invention of the DSC, models were used as a basis to obtain quantitative results from DTA experiments [21,22]. These models have been used for a number of purposes. The most common of which is as the basis for interpretation and analysis of the resulting heat flow rate [2–4,7,8,14,21,22], including the quantification of the energy and onset temperature of transitions, measurement of heat capacities and kinetic analysis. A number of researchers have solved the model systems and compared the results with actual DSC experiments [4,10,11,13,15,17]. Their efforts have aided in understanding the effects of experimental condition variations and the limitations of the assumptions underlying the measurements and the analyses. Models have been used as the basis for determining the heat flow rate baseline during transitions [5,6,8,9]. Accuracy of integration of the heat flow rate peak areas depends on determining the correct heat flow rate baseline. The measured heat flow rate in DSC is distorted by time lags within the measuring system. De-smearing is a post-experiment procedure used to recover the actual sample heat flow. Models have been used to de-smear measured heat flow rates [16–19]. Models have been used to transduce the measured signals, i.e. temperatures and differential temperatures into the desired heat flow rate signals [12,20].

* Fax: +1-302-427-4081.
E-mail address: rdanley@tainst.com (R.L. Danley).
[1] US Patent 6,431,747 additional patents applied for.

0040-6031/$ – see front matter © 2003 Elsevier B.V. All rights reserved.
doi:10.1016/S0040-6031(03)00364-2

In this work, the system of equations used to model the DSC measurement is very similar to those used in the TA Instruments Q1000 DSC to transduce the measured signals. The model system is solved analytically for melting and for solidification of a pure material with super-cooling and compared with experimental results. In both the melt and the solidification, the peaks predicted by the model are quite different from those obtained using the conventional DSC heat flow rate measurement and by previous models. Comparison of the model and experimental results shows that the differences arise from simplifications implicit in DSC heat flow rate measurements that use only the difference between sample and reference calorimeter temperatures. A new DSC heat flow rate measurement method [20] that avoids the simplifications gives results that agree very well with those of the model.

2. DSC model equations

The dynamic behavior of the DSC is simulated by a system of linear first-order differential equations with constant coefficients. They are based on the lumped heat capacity method that represents heat exchange by a network of thermal resistances and heat capacities [23]. This type of model, also known as an electrical analog, is used in all of the references cited here. Constant coefficients imply that thermal conductivity and heat capacity of the elements of the system are independent of temperature. Because those material properties change very slowly with temperature, limiting the temperature range of the solution allows that simplification to be applied and an explicit solution to be found without introducing significant errors. Three differential equations are used to represent the sample calorimeter, one each for the sample, the pan and the calorimeter. Two differential equations are used for the reference calorimeter, one each for the calorimeter and the empty pan. Fig. 1 shows the analogous electrical network. There are no thermal resistances between the sample and reference calorimeters or their pans. This model is only applicable to DSCs where there is negligible heat exchange between the sample and reference calorimeters or their pans. It is not suitable for disk type DSCs that require a thermal resistance joining the sample and reference calorimeters [3,10,11,14–17]. A thermal resistance and a heat capacity represent each calorimeter. Subscripts ‘s’ and ‘r’ indicate sample and reference. The heat capacity of the calorimeter is not included in several of the previous models, limiting their ability to correctly represent the instrument response at the beginning and end of a transition [4,10,11,13]. Pans are represented by a heat capacity, they exchange heat with their respective calorimeters via thermal resistances that simulate the thermal contact resistances between them and the DSC. Subscripts ‘ps’ and ‘pr’ indicate sample and reference pans. The sample is represented by a heat capacity C_{ss} and exchanges heat with the pan via a thermal contact resistance R_{ss}. T_0 is the temperature of the DSC

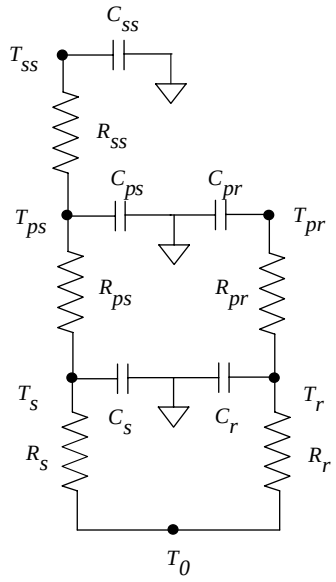

Fig. 1. DSC thermal model. *T*, *R*, *C* are temperatures, thermal resistances and heat capacities. Subscripts ‘s’, ‘r’, ‘ps’, ‘pr’, ‘ss’ indicate sample and reference calorimeters, sample and reference pans and sample.

oven. The model does not include thermal resistance elements representing direct heat exchange between the pans and the DSC enclosure as in other models [10,11,15] because those thermal resistances are very large by comparison with the other thermal resistances in the model, consequently the heat exchanged is very small by comparison with others in the model.

The differential equations for the sample calorimeter are obtained by performing a heat balance on each of the model nodes, giving:

$$\frac{dT_s}{dt} = -T_s\left(\frac{1}{C_s R_s} + \frac{1}{C_s R_{ps}}\right) + \frac{T_{ps}}{C_s R_{ps}} + \frac{T_0}{C_s R_s} \quad (1)$$

$$\frac{dT_{ps}}{dt} = \frac{T_s}{C_{ps} R_{ps}} - T_{ps}\left(\frac{1}{C_{ps} R_{ps}} + \frac{1}{C_{ps} R_{ss}}\right) + \frac{T_{ss}}{C_{ps} R_{ss}} \quad (2)$$

$$\frac{dT_{ss}}{dt} = \frac{T_{ps}}{C_{ss} R_{ss}} - \frac{T_{ss}}{C_{ss} R_{ss}} \quad (3)$$

The differential equations for the reference calorimeter are:

$$\frac{dT_r}{dt} = -T_r\left(\frac{1}{C_r R_r} + \frac{1}{C_r R_{pr}}\right) + \frac{T_{pr}}{C_r R_{pr}} + \frac{T_0}{C_r R_r} \quad (4)$$

$$\frac{dT_{pr}}{dt} = \frac{T_r}{C_{pr} R_{pr}} - \frac{T_{pr}}{C_{pr} R_{pr}} \quad (5)$$

The DSC oven temperature T_0 is an independent function of time that drives the solution. The set of equations above, along with the initial conditions that specify the temperatures at the beginning of the solution are sufficient to describe the DSC. While the complete system includes five equations, the reference and sample calorimeter equations are uncoupled, thus the problem becomes the solution of two sets of three and two differential equations each. The

systems of differential equations are solved explicitly using standard methods [24].

3. Model of fusion

When a pure substance is heated through its melting point, its temperature remains fixed upon reaching its melting point until the latent heat of fusion has been absorbed, after which it begins to heat again. A fusion experiment in a DSC consists of three distinct segments: first is the pre-melt that includes the initiation of heating and establishment of the pre-melt baseline heat flow rate, second is the melt and third is the establishment of the post-melt baseline after the melt is complete. As in previous papers [4,10,11,13,15] the solution for the sample calorimeter is constructed piecewise, consisting of three individual solutions representing each part of the experiment. Because the system of equations for the reference calorimeter is uncoupled from that of the sample calorimeter, a single solution describes the reference calorimeter throughout the entire simulation.

The first segment comprises heating from the initial temperature to the melting point of the sample. The initial conditions for this part of the solution are that all temperatures are set to an initial temperature. The forcing function is the oven temperature, which heats at a constant rate $T_0(t) = T_i + bt$. After sufficient time has elapsed, the stationary solution is reached and all temperatures increase at the same rate as the oven and lag T_0 with constant offsets that depend upon the heating rate and the thermal resistances and heat capacities of the system. The stationary part of the solution is the pre-melt baseline heat flow rate, which is used in DSC to measure the sample heat capacity. The duration of the pre-melt segment can be found by solving the sample temperature equation to find the time that the sample reaches its melting temperature.

The second part of the solution is the melt, during which the sample temperature remains at the melting point until the heat of fusion is absorbed. For this part of the simulation the sample calorimeter model is changed. The sample temperature T_{ss} is fixed at the melting temperature, which reduces the system of sample calorimeter equations to second order. The sample calorimeter and pan temperatures at the end of the pre-melt solution are the initial conditions for the melt segment. After the transient part of the solution for this segment has decayed to zero, the particular solution remains and the heating rates become constant, but are found to be different from the heating rate of temperature T_0. The heating rates of the sample calorimeter and pan are:

$$b_s = \frac{b(R_{ps} + R_{ss})}{R_s + R_{ps} + R_{ss}} \tag{6}$$

$$b_{ps} = \frac{bR_{ss}}{R_s + R_{ps} + R_{ss}} \tag{7}$$

This segment persists until the sample has absorbed the heat of fusion. Its duration is found by integrating the sample heat flow rate and setting it equal to the product of the sample mass and the latent heat of fusion

$$m_{ss}h_f = \int_{t_p}^{t_l} \dot{q}_{ss}\,\mathrm{d}t \tag{8}$$

The resulting equation is solved for t_l, the time at the end of the melt, t_p is the time at the end of the first segment. The heat flow to the sample is just that which passes through the thermal resistance between pan and sample:

$$\dot{q}_{ss} = \frac{T_{ps} - T_m}{R_{ss}} \tag{9}$$

The final part of the solution is the return to baseline after the sample is completely melted. The solution is identical to that of the first segment, except that the initial conditions are the sample melting temperature and the sample calorimeter and pan temperatures at the end of the melting segment.

4. Model of solidification with super-cooling

Many materials exhibit the phenomena of super-cooling during solidification, where freezing begins at temperatures below their melting point because of the time required for crystals to nucleate after the melting point is reached. Once nucleation begins heat is liberated raising the temperature of the material and if the degree of super-cooling is not too great the sample may regain its melting temperature where it remains until the heat of fusion is released [25]. In some instances the degree of super-cooling is sufficiently large that the heat of fusion is released before the melting point is regained. That case is not considered here, although it could be solved easily using the method described here. The solution is taken piecewise and is similar to the melting solution, comprising three segments.

The first segment is similar to the first melting segment, except that the DSC is cooled from an initial temperature above the melting point and the segment terminates when the sample reaches a specified temperature below the melting point. The duration of the first segment can be found by solving the sample temperature equation to find the time that the sample reaches the temperature at the beginning of crystallization.

At the beginning of the solidification segment, the sample temperature is changed from T_c, the temperature at which crystallization commences to the melting temperature T_m where it remains until the heat of fusion is released. The step change of sample temperature was used in more simplified models of solidification with super-cooling [4,13]. Initial conditions are the sample calorimeter and pan temperatures at the end of the first segment. As in the melting simulation, the calorimeter model is reduced to second order by fixing the sample temperature. The duration of this

segment is again found by determining the time when the entire heat of fusion of the sample is released. Because of the step change of sample temperature, the change in sensible heat in the sample must be included in the energy balance. The resulting equation is solved for t_s, the time at the end of solidification

$$-m_{ss}h_f + C_{ss}(T_m - T_c) = \int_{t_p}^{t_s} \dot{q}_{ss}\,dt \tag{10}$$

Finally, the last segment of the solidification simulation is the return to baseline, which is identical to that of the melt except that the initial conditions are the temperatures at the end of the solidification. The solution for the reference calorimeter is identical to that for the melt except that the initial temperatures are above the melting point and the heating rate is negative. It persists throughout the simulation of solidification.

5. DSC heat flow rate measurement

The heat flow rate measurement in the vast majority of DSCs is the temperature difference between the sample and reference calorimeters divided by a temperature-dependent thermal resistance

$$\dot{q} = \frac{T_r - T_s}{R(T)} \tag{11}$$

This measurement is based on a number of simplifying assumptions: heat flow rates are constant, only the thermal resistance between the furnace and sample is taken into account, pan and calorimeter heat capacities are ignored, measured temperature equals sample temperature and there is no heat exchange with the surroundings [26]. During a transition the sample and reference heating rates are generally not the same. Strictly speaking this measurement equation is not applicable during transitions, thus the heat flow rate signal is smeared [26].

Recently, a new method of heat flow rate measurement was developed that greatly reduces the smearing [20]. Eq. (1), the sample calorimeter heat balance equation is solved for the heat flow rate between the sample calorimeter and pan

$$\dot{q}_s = \frac{T_0 - T_s}{R_s} - C_s\frac{dT_s}{dt} \tag{12}$$

Similarly, Eq. (4) is solved for the heat flow rate between the reference calorimeter and pan

$$\dot{q}_r = \frac{T_0 - T_r}{R_r} - C_r\frac{dT_r}{dt} \tag{13}$$

Performing a heat balance on the sample pan gives the equation for the heat exchange between the sample and its pan

$$\dot{q}_{ss} = \dot{q}_s - m_{ps}c_{pan}\frac{dT_{ps}}{dt} \tag{14}$$

If the reference pan is empty, the specific heat capacity of the pan may be found from the reference heat flow rate

$$c_{pan} = \frac{\dot{q}_r}{m_{pr}(dT_{pr}/dt)} \tag{15}$$

Which upon substitution into Eq. (14) gives the equation for the heat flow rate between the sample and its pan, which is the objective of the measurement

$$\dot{q}_{ss} = \dot{q}_s - \dot{q}_r\frac{m_{ps}(dT_{ps}/dt)}{m_{pr}(dT_{pr}/dt)} \tag{16}$$

The sample and reference pan temperatures may be obtained using expressions for heat exchange through the contact resistance between sample and reference pans and calorimeters

$$T_{ps} = T_s - \dot{q}_s R_{ps} \tag{17}$$

$$T_{pr} = T_r - \dot{q}_r R_{pr} \tag{18}$$

The sample and reference calorimeter thermal resistances and heat capacities used in Eqs. (12) and (13) are found using a two-step calibration procedure. In the first step, the empty DSC is heated at constant rate and the second step is a repeat of the first except that sapphire samples without pans are placed on both the sample and reference. Details of the analysis may be found elsewhere [20]. Pan contact resistances required for use in Eqs. (17) and (18) are obtained from a semi-empirical contact resistance function [20]. Three measurements are used to obtain the required temperatures and temperature differences: ΔT the difference between sample and reference calorimeter temperatures, ΔT_0 the temperature difference across the sample calorimeter thermal resistance and T_0 the temperature at the base of the sensor assembly.

6. Model computations

Computations were performed for indium samples with heating rate of 10 °C/min at 0.1 s intervals, matching the data collection rate of the DSC. The melting point of indium was taken to be 156.6 °C, the heat of fusion of indium was 28.71 kJ/kg and the specific heat capacity was 234 J/kg °C for both the solid and liquid states. Values for thermal resistances and heat capacities for the sample and reference calorimeters are taken from the DSC sensor thermal resistance and heat capacity calibration results at 156 °C and the pan contact resistance is the value at 156 °C used by the DSC software to determine the pan temperature. The crystallization temperature for each model simulation is chosen to agree with the experimental DSC result. Mathcad®, a general-purpose mathematics program from Mathsoft Engineering and Education Inc. was used for all computations.

Contact resistance between the sample and the pan is determined from the experimental results as follows.

Differentiation of Eq. (9) gives the slope of the heat flow rate during the melt:

$$\ddot{q}_{ss} = \frac{\dot{T}_{ps}}{R_{ss}} \tag{19}$$

During the constant heating rate portion of either the melt or the solidification, the heating rate of the sample pan is given by Eq. (7). Substitute into Eq. (19):

$$\ddot{q}_{ss} = \frac{b}{R_s + R_{ps} + R_{ss}} \tag{20}$$

This result is well known as noted by other authors [4,5,8,10] and shows that the slope of the heat flow rate during the constant heating rate portion of the melt is equal to the quotient of the oven heating rate and the total thermal resistance between the sample and the oven. The thermal resistance between pan and sample is found from this:

$$R_{ss} = \frac{b}{\ddot{q}_{ss}} - R_s - R_{ps} \tag{21}$$

The heat flow rate may be calculated in a number of ways, depending upon the desired result. The conventional DSC heat flow is calculated using Eq. (11). Eq. (16) may be used along with Eqs. (12), (13), (17) and (18) for comparison with the experimental results obtained using the TA Instruments Q1000 DSC. The heat flow rate through the contact resistance between sample and pan may be calculated

$$\dot{q}_{ss} = \frac{T_{ps} - T_{ss}}{R_{ss}} \tag{22}$$

This last result is very useful because it is the actual sample heat flow rate and not the result of a measurement as in the other two sample heat flow rate equations. This equation will be used below to explain the observed heat flow results. It is noted that when the model results are used to calculate the sample heat flow rates using Eq. (22) or Eqs. (12), (13) and (16)–(18) they are identical.

7. Experimental procedure

Experiments were performed using a TA Instruments Q1000 DSC with RCS mechanical cooling system. DSC thermal resistances and heat capacities were calibrated at a heating rate of 10 °C/min between 80 and 220 °C. Single point temperature and enthalpy calibration was done using indium. Standard crimped aluminum pans were used for all samples and the DSC cell was purged with nitrogen. Three indium samples were used, 2.09, 10.87 and 58.23 mg, all were flattened before being placed in the pans. The thermal program comprised: equilibrate at 120 °C, hold isothermal for 5 min, heat 10 °C/min to 180 °C, equilibrate, hold isothermal for 5 min, cool 10 °C/min to 120 °C. Conventional DSC heat flow rate measurement using Eq. (11) and the improved heat flow rate measurement using Eqs. (12), (13) and (16)–(18) are collected along with sample sensor and pan temperatures.

8. Comparison of model and experimental results

Model solutions are overlaid on the results from the DSC experiments by aligning the sample pan temperatures, T_{ps} in the model. Both model and experimental results are plotted versus experiment time. In all plots, DSC improved heat flow rate uses the method of Eqs. (12), (13) and (16)–(18) and DSC conventional heat flow rate uses Eq. (11). Model sample heat flow rate is calculated from the model result using Eq. (22) and model conventional heat flow rate uses Eq. (11).

Fig. 2 shows the comparison of the 10.87 mg melt plotted versus time. The model and DSC conventional heat flow rates, DSC improved heat flow rate and model sample heat flow rate are shown. The conventional DSC and model heat flow rates agree quite well and have the expected peak shape. The DSC improved heat flow rate and the model sample

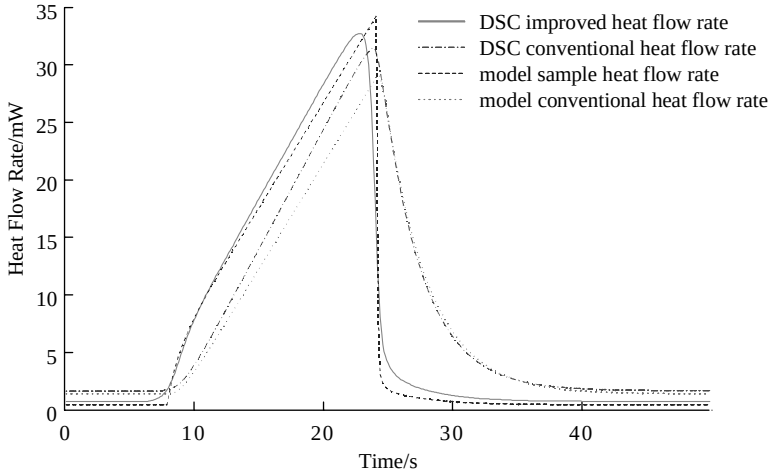

Fig. 2. Heat flow rates for 10.87 mg indium melt at 10 °C/min. DSC improved heat flow rate equations (12), (13) and (16)–(18); DSC conventional heat flow rate equation (11); model sample heat flow rate equation (22); model conventional heat flow rate equation (11).

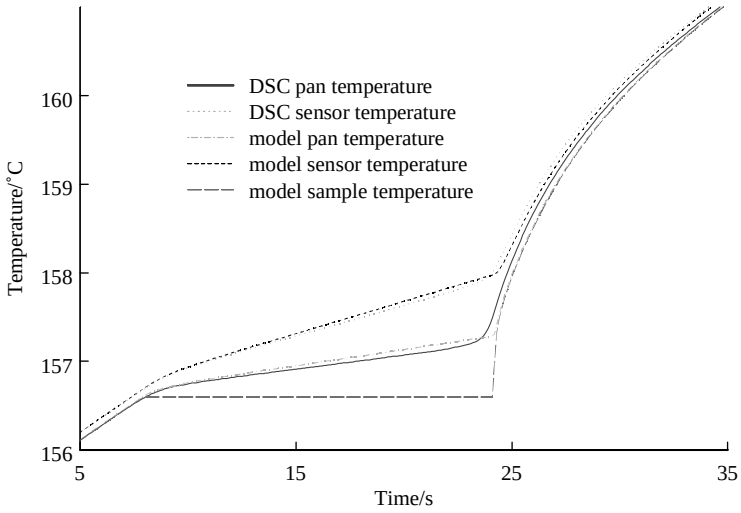

Fig. 3. Temperatures for 10.87 mg indium melt at 10 °C/min. DSC pan and sensor temperatures, model pan, sensor and sample temperatures.

heat flow rate agree well with each other however, the peaks are quite different from the conventional heat flow rates. By comparison with the conventional heat flow rates, the other two heat flow rates have differently shaped onsets, higher and earlier peak heat flow rate and much more rapid return to baseline. The difference in onset shape may be explained by considering the rate of change of the heat flow rate between the sample and pan. Eq. (22) is differentiated with respect to time to obtain the slope of the sample heat flow rate

$$\ddot{q}_{ss} = \frac{\dot{T}_{ps} - \dot{T}_{ss}}{R_{ss}} \tag{23}$$

Fig. 3 shows the model and the DSC sample sensor and pan temperatures and the model sample temperature. The model and DSC sensor and pan temperatures agree very well, while the model sample temperature follows the idealized behavior. Consider the slope of the heat flow rate as given by Eq. (23). Prior to the melt, both the sample and pan heat at the same rate, consequently the slope of the heat flow rate is zero. At the instant the melt commences, the derivative of the sample temperature becomes zero and the slope of the sample heat flow rate is proportional to the heating rate of the sample pan. At the melt onset the sample pan heating rate is still equal to the scanning rate and as the melt continues the heating rate of the sample pan decreases until it reaches a constant value given by Eq. (7) that is less than the scanning rate. Thus, the slope of the heat flow rate should be maximum at the onset and decrease until it reaches a constant value which it maintains until the melt is complete. The behavior predicted by the model is confirmed by the DSC improved heat flow rate measurement. Claudy et al. showed the same onset in a de-smeared 40.34 mg indium melt [16, Fig. 2] although they made no comment regarding the difference between it and the conventional smeared result. More simplistic models of the heat flow rate show the onset as a discontinuous change of slope from zero to that of the constant heating rate condition [4,7,8,13]. Although that response is apparently confirmed by the appearance of the melt onset as measured using conventional DSC, it is the result of using the simplified heat flow rate measurement of Eq. (11) that neglects the heating rate differences between the sample and reference sensors and pans which occur during a melt. The improved heat flow rate measurement includes these effects and measures the sample heat flow rate more correctly. Fig. 2 also shows that the baseline heat flow rates before and after the melt agree well between the DSC and the model for both heat flow rate signals. However, there is a significant offset between the improved and conventional measurements resulting from the conventional assumption that the DSC is perfectly symmetric. In this case, where the sample has very low specific heat capacity, the error resulting from this simplification is larger than the heat flow rate signal due to the sample heat capacity.

Fig. 4 shows the model and DSC heat flow rate signals for the 2.09 mg indium melt. In general, all of the comments made for the 10.87 mg sample pertain, except that in this instance the melt is complete before the sample reaches a constant heating rate. While that is clear from the improved heat flow rate, the conventional DSC result may be interpreted as having reached the constant heating rate condition. This may be important in analyses where the onset slope of the heat flow rate signal is used, for instance in purity analysis. Caution should be used to be sure that the constant heating rate condition is achieved. Comparison of Figs. 2 and 4 show that the melt onsets are nearly identical, and reflect only the characteristics of the sample sensor, pan, associated thermal resistances and programmed heating rate.

In the solidification of 10.89 mg of indium shown in Fig. 5, both the DSC improved heat flow rate and the model sample heat flow rate are strikingly different from the conventional heat flow rate signals. As in the melt, the peak at the end of the transition is higher and occurs earlier and the return to baseline after the transition is complete is faster using the new heat flow measurement. The strong initial exothermic

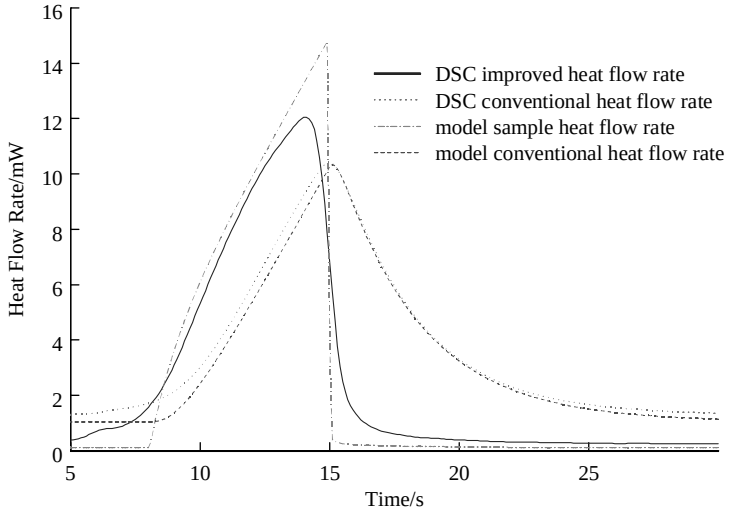

Fig. 4. Heat flow rates for 2.09 mg indium melt at 10 °C/min. DSC improved heat flow rate equations (12), (13) and (16)–(18); DSC conventional heat flow rate equation (11); model sample heat flow rate equation (22); model conventional heat flow rate equation (11).

peak is explained by considering the sample and pan temperatures and the heat exchange between them as expressed by Eq. (22). Fig. 6 shows the model and the DSC sample pan and sample sensor temperatures and the model sample temperature. Model and DSC sample pan and sensor temperatures agree well while the model sample temperature follows the idealized behavior. Because the pan and sensor temperatures respond to changes in sample temperature, it is clear that the DSC temperatures are the result of the sample temperature increasing very rapidly to the melting temperature once crystallization begins, like the step change of the model sample temperature. The model temperatures show that because the sample heats rapidly up to the melting point, a large temperature difference develops between the pan and the sample causing a very large heat flow rate, quickly reaching a maximum and generating the sharp initial peak heat flow rate. As the sample pan temperature increases the heat flow rate decays to a local minimum as the heating rates of sample calorimeter, pan and sample become constant. A similarly large temperature difference occurs between the DSC sample and pan and is responsible for the sharp peak immediately after the onset. During the constant heating rate part of the solidification, the difference between sample and pan temperature increases gradually resulting in a heat flow rate with the same slope as the melt until solidification is complete at the second heat flow peak, after which it decays rapidly and returns to the baseline. In conventional DSC the initial peak is not observed because the differences in heating rates between sample and reference calorimeters and pans are neglected, i.e. smearing of the heat flow rate signal.

Simplified models of the solidification process [4,13] have shown the heat flow rate during solidification with super-cooling as a step change followed by a linear increase

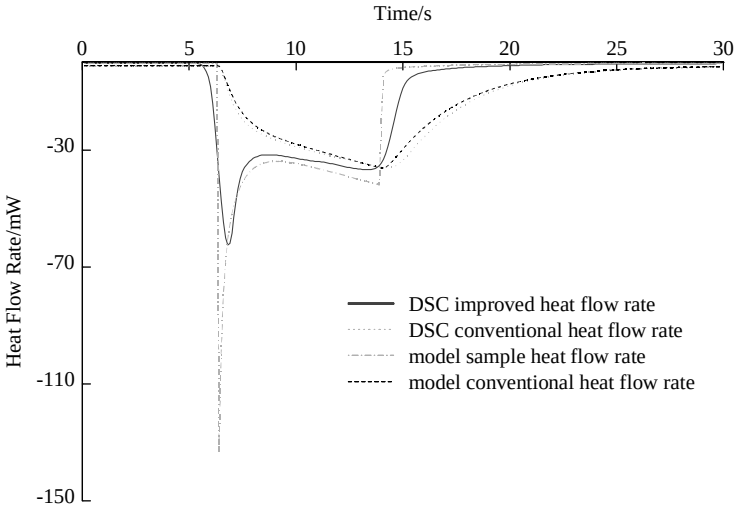

Fig. 5. Heat flow rates for 10.87 mg indium solidification at 10 °C/min. DSC improved heat flow rate equations (12), (13) and (16)–(18); DSC conventional heat flow rate equation (11); model sample heat flow rate equation (5); model conventional heat flow rate equation (11).

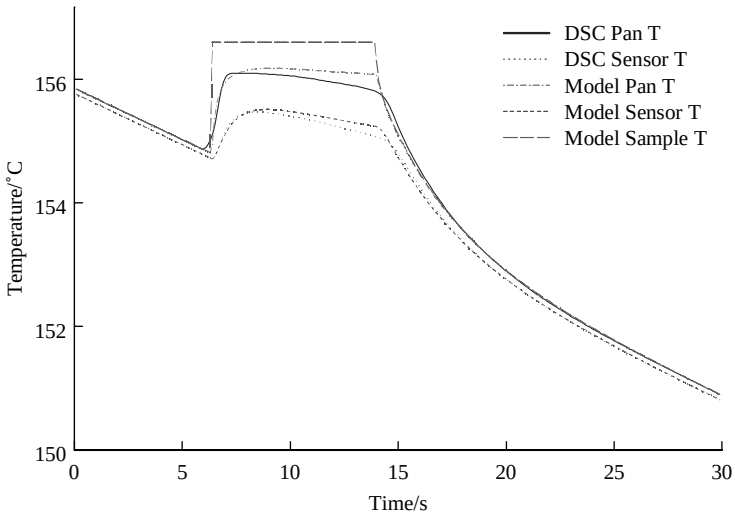

Fig. 6. Temperatures for 10.87 mg indium solidification at 10 °C/min. DSC pan and sensor temperatures, model pan, sensor and sample temperatures.

to the peak at the end of solidification and an exponential return to baseline. Both are based upon the sample temperature changing instantly from the super-cooled value to the melting point, just as in the model used here. In those models only the thermal resistance between the oven and the sample are considered and the heat capacities of the pan and the calorimeter are ignored. Because of those simplifications, they are incapable of showing the initial heat flow peak resulting from rapid heating of the sample. However, once the transient part of the experiment is completed and the stationary condition is obtained, the linear increase in heat flow rate predicted by the simple models is obtained in both the model presented here and the actual DSC experiment. This behavior can be seen more clearly in Fig. 7, showing the solidification results for a 58.32 mg indium sample. The initial peak is present while the constant heating rate portion of the solidification is much longer, reaching a maximum heat flow rate considerably greater than the initial peak. Fig. 8 shows the same temperatures during the transition as in Figs. 3 and 6. In this case, the final peak, marking the end of the solidification is greater than the initial solidification peak because the sample takes much longer to solidify owing to its greater mass and thus, a greater temperature difference is created between the sample and the pan.

At both the beginning and end of the transitions, the DSC result is not as abrupt as the model. Possible explanations are that the model is too simplified or that the sample temperature is not uniform. If the sample temperature is not uniform during the transition because of heat exchange effects, the resulting heat flow rate signal will not change abruptly as in the model. It is likely that such small temperature inhomogeneities exist and contribute to the deviation from idealized behavior.

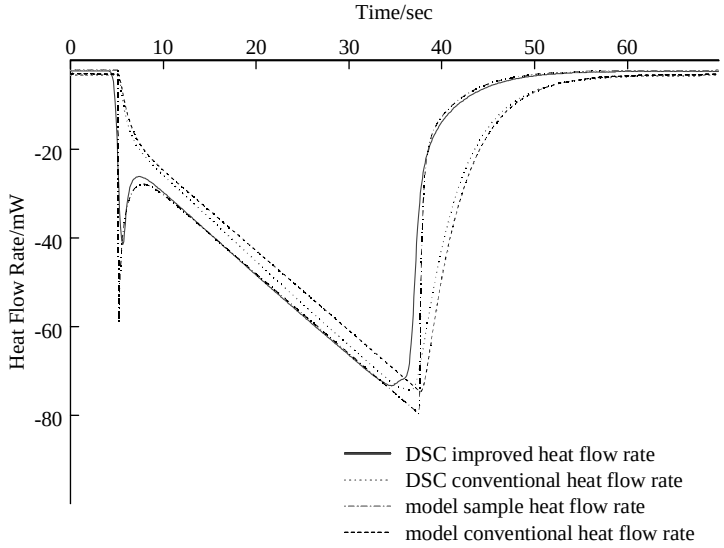

Fig. 7. Heat flow rates for 58.23 mg indium solidification at 10 °C/min. DSC improved heat flow rate equations (12), (13) and (16)–(18); DSC conventional heat flow rate equation (11); model sample heat flow rate equation (22); model conventional heat flow rate equation (11).

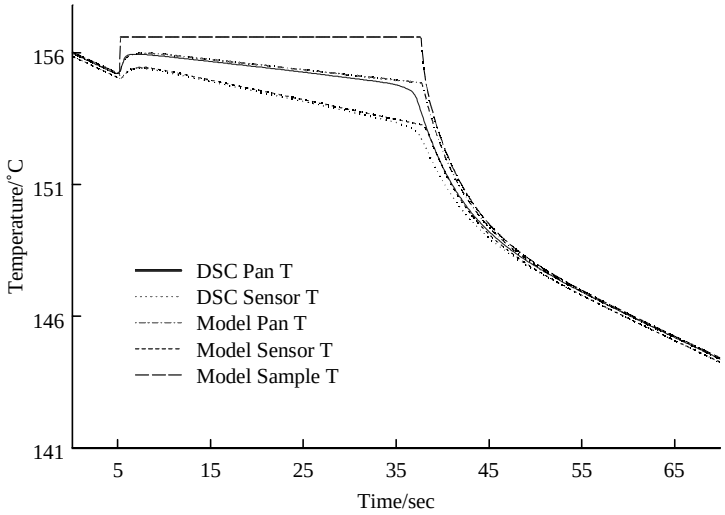

Fig. 8. Temperatures for 58.23 mg indium solidification at 10 °C/min. DSC pan and sensor temperatures, model pan, sensor and sample temperatures.

9. Conclusions

A model system of linear constant coefficient first-order differential equations is solved to simulate a DSC for fusion and solidification with super-cooling. In both the melt and solidification experiments, the peak shape predicted by the model for the heat flow rate between the sample and pan is considerably different from that obtained using the conventional DSC heat flow rate measurement. The model results are compared with results for the same experiments performed using a TA Instruments Q1000 DSC. Model and experiment conventional DSC heat flow rate signals based on the difference between the sample and reference calorimeter temperatures are compared, as were the improved heat flow rate and the model sample heat flow rate. Experimental and model results agreed very well for two melt and two solidification experiments. The conventional DSC heat flow rate measurement using only the difference between the sample and reference calorimeters is unable to give the correct heat flow rate during first-order transitions because the signal is smeared. First-order transitions are correctly displayed by the improved heat flow rate measurement, which accounts for imbalances and heating rate differences between the sample and reference calorimeters and pans.

References

[1] W. Hemminger, G. Hohne, Calorimetry Fundamentals and Practice, Verlag, Weinheim, 1984, p. 113.
[2] A.P. Gray, in: R.S. Porter, J.F. Johnson (Eds.), Analytical Calorimetry, vol. 1, Plenum Press, New York, 1968, p. 209.
[3] R.A. Baxter, in: R.F. Schwenker, P.D. Garn (Eds.), Thermal Analysis, vol. 1, Academic Press, New York, 1969, p. 65.
[4] J.H. Flynn, in: R.S. Porter, J F. Johnson (Eds.), Analytical Calorimetry, vol. 3, Plenum Press, New York, 1972, p. 17.
[5] W.P. Brennan, B. Miller, J.C. Whitewell, in: R.S. Porter (Ed.), Analytical Calorimetry, vol. 1, Plenum Press, New York, 1970, p. 441.
[6] C. Sandu, D. Lund, Thermochim. Acta 88 (1985) 453.
[7] C. Sandu, R. Singh, Thermochim. Acta 132 (1988) 89.
[8] C. Sandu, R. Singh, Thermochim. Acta 159 (1990) 267.
[9] G. van der Plaats, Thermochim. Acta 72 (1984) 77.
[10] G.-W. Jang, K. Rajeshwar, Anal. Chem. 58 (1986) 416.
[11] G.-W. Jang, K. Rajeshwar, Anal. Chem. 60 (1988) 1003.
[12] M.J. O'Neill, Anal. Chem. 36 (7) (1964) 1238.
[13] M.J. O'Neill, Anal. Chem. 47 (4) (1975) 630.
[14] P. Claudy, J.C. Commercon, J.M. Letoffe, Thermochim. Acta 65 (1983) 245.
[15] P. Claudy, J.C. Commercon, J.M. Letoffe, Thermochim. Acta 68 (1983) 305.
[16] P. Claudy, J.C. Commercon, J.M. Letoffe, Thermochim. Acta 68 (1983) 317.
[17] H.B. Dong, J.D. Hunt, J. Therm. Anal. Catal. 64 (2001) 167.
[18] K.H. Schönborn, Thermochim. Acta 69 (1983) 103.
[19] K.-R. Löblich, Thermochim. Acta 85 (1985) 263.
[20] R.L. Danley, Thermochim. Acta 395 (1–2) (2003) 199.
[21] M. Vold, Anal. Chem. 21 (6) (1949) 683.
[22] H.J. Borchardt, F. Daniels, J. Am. Chem. Soc. 79 (1957) 41.
[23] J.P. Holman, Heat Transfer, 4th ed., McGraw-Hill, New York, 1976, pp. 97–102.
[24] E.D. Rainville, P.E. Bedient, Elementary Differential Equations, Macmillan, New York, 1974.
[25] B. Wunderlich, Thermal Analysis, Academic Press, New York, 1990, pp. 104–106.
[26] G. Höhne, W. Hemminger, H.-J. Flammersheim, Differential Scanning Calorimetry: An Introduction for Practitioners, Springer, Berlin, 1996, pp. 20–24.